Dalton Transactions

ROYAL SOCIETY OF CHEMISTRY

PAPER

View Article Online
View Journal | View Issue

Cite this: *Dalton Trans.*, 2021, **50**, 3874

High denticity oxinate-linear-backbone chelating ligand for diagnostic radiometal ions $[^{111}In]In^{3+}$ and $[^{89}Zr]Zr^{4+}$†‡

Lily Southcott, [a,b] Xiaozhu Wang, [a] Luke Wharton, [a,b] Hua Yang, [b] Valery Radchenko, [b,c] Manja Kubeil, [d] Holger Stephan, [d] María de Guadalupe Jaraquemada-Peláez *[a] and Chris Orvig *[a]

Received 12th December 2020,
Accepted 16th February 2021

DOI: 10.1039/d0dt04230g

rsc.li/dalton

Advances in nuclear medicine depend on chelating ligands that form highly stable and kinetically inert complexes with relevant radiometal ions for use in diagnosis or therapy. A new potentially decadentate ligand, H_5decaox, was synthesised to incorporate two 8-hydroxyquinoline moieties on either end of a diethylenetriamine backbone decorated with three carboxylic acids, one at each N atom of the backbone. Metal complexation was assessed using nuclear magnetic resonance (NMR) spectroscopy and high-resolution mass spectrometry (HR-MS) with In^{3+}, Zr^{4+} and La^{3+}. Solution thermodynamic studies provided the stepwise protonation constants and metal formation constants, indicating a high affinity for both In^{3+} and Zr^{4+} (pIn = 32.3 and pZr = 34.7), and density functional theory (DFT) calculations provided insight into the coordination environments with either metal ion. Concentration dependent radiolabeling experiments with $[^{111}In]InCl_3$ and $[^{89}Zr]ZrCl_4$ showed promise as quantitative radiolabeling (>95%) occurred at micromolar concentrations, under mild, near-physiological conditions of pH 7 and room temperature for 30 minutes. Serum stability of both radiometal complexes was investigated and the $[^{111}In]In$(decaox) complex remained 91% intact after 24 hours while the $[^{89}Zr]Zr$(decaox) complex was 86% intact over the same time, comparable to other chelating ligands previously assessed with the same methods. The high radiolabeling yields, limited serum protein transchelation and structural insight of the $[^{89}Zr]Zr$(decaox) complex suggest a promising fit between the oxinate-containing ligand and the Zr^{4+} ion, setting the stage for further investigations with a functionalised version of the chelator for its potential in PET imaging.

Introduction

Nuclear medicine comprises diagnosis and treatment of disease by exploiting the decay properties of radioactive nuclides. Radionuclides decay in different modalities, giving rise to diagnostic techniques based on γ-detection, positron emission tomography (PET) and single photon emission computed tomography (SPECT), and therapies based on β^- or α particles, or Auger electrons.[1–3] As the accessibility to new isotopes is burgeoning with more and better cyclotrons, as well as generators and other production methods being implemented, the type and number of isotopes available is dramatically increasing. To harness the diagnostic or therapeutic ability of a radioactive isotope, it must be safely administered and delivered to its biological target, otherwise unwanted adverse effects become prominent. Central to development in metalloradiopharmaceuticals is the coordinating ligand that is designed to chelate a radiometal ion to form a stable complex that will not dissociate once administered.[2]

Chelators are often designed specifically for the metal ion of interest – the size, charge and decay properties of the radiometal ion itself will influence the stability and inertness of the overall coordination complex.[4] When comparing ligands for stable metal complexes in radiopharmaceuticals, a balance between rapid complexation and kinetic inertness is highly desired. One of the most commonly used in metalloradiopharmaceuticals is the macrocyclic chelator DOTA (1,4,7,10-tetraazacyclododecane-1,4,7,10-tetraacetic acid) (Fig. 1), which forms

[a]*Medicinal Inorganic Chemistry Group, Department of Chemistry, University of British Columbia, 2036 Main Mall, Vancouver, British Columbia V6T 1Z1, Canada. E-mail: orvig@chem.ubc.ca, mdgjara@chem.ubc.ca*
[b]*Life Sciences Division, TRIUMF, 4004 Wesbrook Mall, Vancouver, British Columbia, V6T 2A3, Canada*
[c]*Department of Chemistry, University of British Columbia, 2036 Main Mall, Vancouver, British Columbia V6T 1Z1, Canada*
[d]*Institute of Radiopharmaceutical Cancer Research, Helmholtz-Zentrum Dresden Rossendorf, Bautzner Landstrasse 400, 01328 Dresden, Germany*
†Invited for the 50th volume of *Dalton Trans.*
‡Electronic supplementary information (ESI) available. See DOI: 10.1039/d0dt04230g

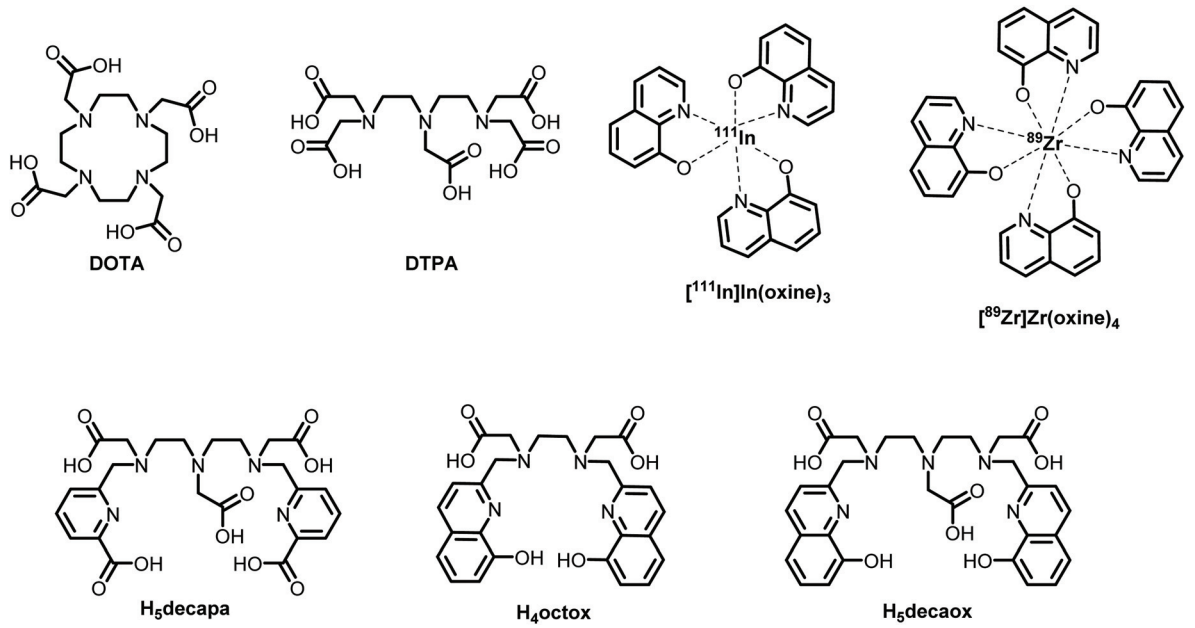

Fig. 1 Chemical structures of selected chelators and complexes.

highly inert complexes but often requires harsh radiolabeling conditions (high temperatures, long incubation times) that are not suitable for bioconjugates.[5,6] DTPA (diethylenetriamine pentaacetic acid) is an exemplary acyclic chelator with five carboxylic acid moieties attached through the linear diethylenetriamine backbone. It radiolabels metals quickly (under 15 minutes) in mild conditions (room temperature (RT)); however, it has inferior *in vivo* stability compared to the macrocycle DOTA.[5] While both ligands or their targeting derivatives are in standard use, combining the rapid complexation of DTPA with *in vivo* stability of DOTA would yield a novel chelator of significant importance to metalloradiopharmaceuticals. To achieve such a balance between fast complexation and *in vivo* inertness, non-macrocylic ligands with rigid functional groups or backbones have recently been a focus when combined with 8-hydroxyquinoline as a chelating moiety.[7–11]

8-Hydroxyquinoline (8-HQ, oxine) is a small, bicyclic molecule that has been used extensively in analytical chemistry,[12,13] medicinal chemistry and nuclear medicine.[14–17] As an imaging agent in nuclear medicine, metal–oxinate complexes typically have been used as ionophores: lipophilic, low denticity and *meta*-stable complexes to allow the transport of a metal ion into cells. The most widely used example is the tris ligand complex, [^{111}In]In(oxinate)$_3$ (Fig. 1),[18–21] which has been used for decades to radiolabel leukocytes for SPECT imaging of inflammation and infection. Similarly reported are M(oxinate) complexes of various radiometals: [^{52}Mn]Mn(oxinate)$_2$,[22] [^{68}Ga]Ga(oxine)$_3$,[23] and [^{89}Zr]Zr(oxinate)$_4$.[24,25] [^{89}Zr]Zr(oxinate)$_4$ has been used increasingly in mouse models for tracking of cell-based therapies,[24] liposomes,[26] and bone marrow[27] – this leads to applications in PET imaging of cancer, arthritis and acute bone injury response. Both [^{111}In]In^{3+} and [^{89}Zr]Zr^{4+} provide interesting radiometal isotopes for their respective imaging modalities, SPECT and PET.[3,4] [^{111}In]In^{3+} is regularly cyclotron-produced, widely commercially available and has useful properties for SPECT imaging, including a half-life ($t_{\frac{1}{2}}$) of 2.8 days, and average E_γ = 171 and 245 keV.[4] Interest in developing PET probes with [^{89}Zr]Zr^{4+} has increased dramatically in the last few years as its suitability for antibody targeting radiopharmaceuticals is realised: a mid-range half-life ($t_{\frac{1}{2}}$ = 78 h, long for a positron emitter) and low energy ($E_{\beta+}$ = 396 keV) plus availability and ease of production on medical cyclotrons.[3,28,29]

Combining the idea of non-macrocyclic chelators for rapid complexation and high kinetic inertness with the oxinate moiety found in ionophoric complexes, several multidentate ligands containing oxine groups have recently been reported by us – including H$_2$hox,[7] H$_4$octox,[8] H$_4$bispox,[9] H$_3$glyox,[10] and H$_2$*CHX*hox,[11] which are six- to eight-coordinating ligands that radiolabel at high efficiencies with various metal ions including [^{68}Ga]Ga^{3+}, [^{111}In]In^{3+}, and [^{177}Lu]Lu^{3+}. To exploit the versatility of the 'ox' family of ligands and to accommodate larger metal ions with higher coordination numbers, a new, oxine-containing ligand was conceived based upon the diethylenetriamine backbone of DTPA, and the utility of our previously reported H$_5$decapa.[30] Incorporating the bicycle oxine as arms for the diethylenetriamine backbone could be beneficial to enhance the rigidity of the ligand and in turn improve the stability of its metal complexes.

The potentially decadentate ligand, H$_5$decaox (Fig. 1), was synthesised and its utility was tested by selecting metal ions by charge (3+ *vs.* 4+) and size to identify any coordination preferences, consistent with the availability of relevant radioisotopes. In^{3+} is a metal ion with borderline hardness, while the smaller

Zr^{4+} prefers hard, anionic donors, allowing for a comparison to be made upon complexation with H_5decaox to understand its coordination preferences. Further, with increasing interest in radiometals for therapy, [^{225}Ac]Ac^{3+} ($t_{\frac{1}{2}}$ = 9.9 days, α-decay)[31] and nonradioactive surrogate La^{3+} were also chosen to investigate the potential of the large backbone of H_5decaox to accommodate larger metal ions.

Results and discussion

Synthesis and characterisation

Starting from diethylenetriamine, H_5decaox was synthesised in five steps with an initial nosyl protection step and alkylation with *tert*-butyl bromoacetate (Scheme 1). After the nosyl deprotection *via* thiophenol, the product was alkylated with the synthesised building block, 2-(bromomethyl)quinoline-8-ol. Final ligand deprotection proceeded with 6 M HCl and the desired product was purified *via* reverse-phase C18 automated column chromatography. Although the overall yield is only 8.4%, efforts to improve yields and solubility with a hydroxyl protecting group for 8-hydroxyquinoline derivatives were attempted (acetate, *tert*-butyldimethylsilyl, benzene sulfonyloxy). While the protecting groups improved ligand solubility, they ultimately impeded the succeeding reactions or were cleaved during alkylation steps, leading to a mixture of partially protected products and more complicated purification steps. Proceeding without protecting groups and continuing to the final H_5decaox deprotection without purification simplified synthetic procedures and optimised yield. This resulted in a ligand similar to the acyclic DTPA, exchanging the two flexible carboxylic acid moieties on either end for more rigid, 8-hydroxyquinoline arms. Compared to previous 'ox' ligands, this is the highest denticity example, and the most complicated to synthesise.

Metal complexation

Metal complexation of H_5decaox with $In(ClO_4)_3$, $La(NO_3)_3$, and $ZrCl_4$ was achieved and characterised with ^{1}H NMR, ^{1}H–^{1}H correlation spectroscopy (COSY) and high resolution mass spectrometry (HR-MS). All complexes were confirmed by HR-MS, but the inherent insolubility of the complexes limited complete structural characterisation. The ^{1}H NMR of In(decaox) indicates a metal complex species with one oxinate arm metal-bound and one oxine unbound (Fig. 2). This is evinced by five sharp, resolved peaks in the aromatic region (7.58–9.12 ppm) representing the metal bound 8-hydroxyquinolinate, while the remaining small, broad aromatic peaks (6.66–7.09 ppm) correspond to the more fluxional unbound arm. The proton correlations of the five bound aromatic protons are clear in the COSY spectrum (Fig. 2C), while the remaining peaks of the unbound arm are found overlapping at 7.58 ppm, indicating the two distinct hydroxyquinoline arm environments and accounting for all expected protons in the aromatic region. Further, the diastereotopic splitting of the methylene protons of the acetate arms and the additional splitting of the diethylene backbone protons provides evidence of one isomer with minimised fluxional interconversion as

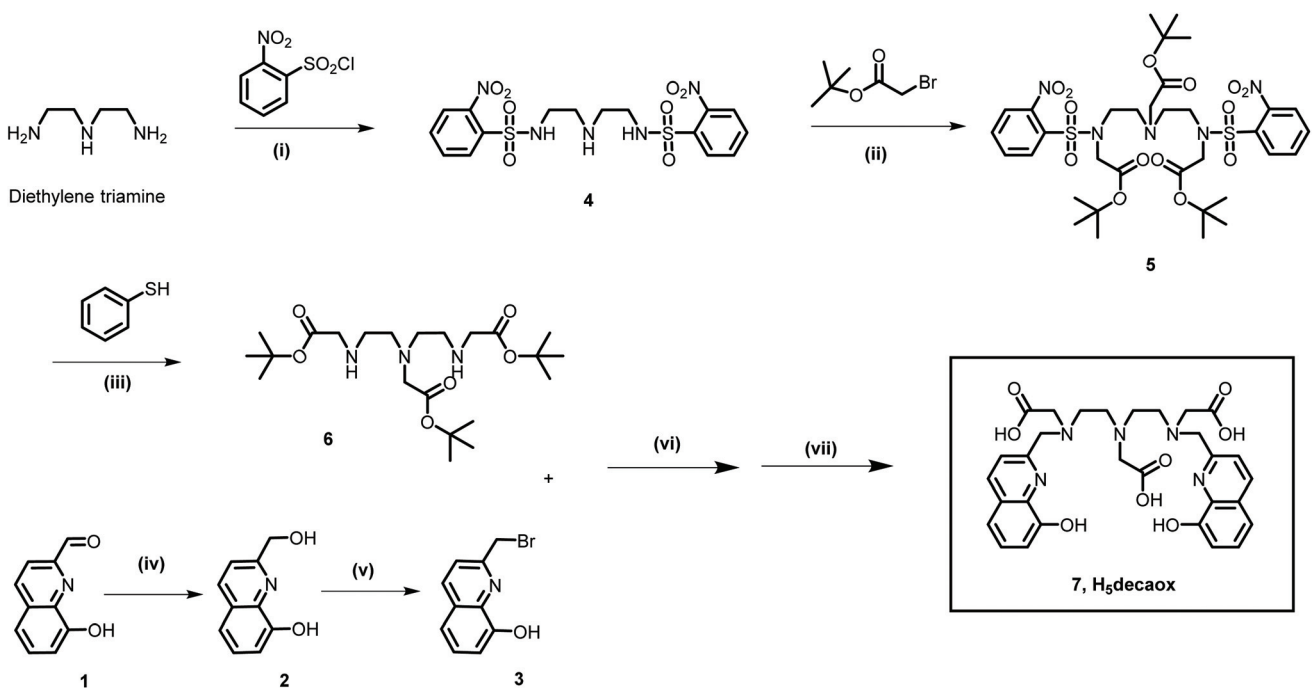

Scheme 1 H_5decaox synthesis, reagents and conditions (i) Na_2CO_3, THF, 0 °C → RT, 18 h, 52%, (ii) K_2CO_3, CH_3CN, reflux, 24 h, 96%, (iii) K_2CO_3, CH_3CN, reflux, 24 h, 56%, (iv) $NaBH_4$, MeOH, 0 °C → RT, 18 h, 75%, (v) PBr_3, CH_3CN, 0 °C, 5 h, 74%, (vi) K_2CO_3, CH_3CN, reflux, 24 h and (vii) 6 M HCl, THF, 50 °C, 18 h (30% over 2 steps).

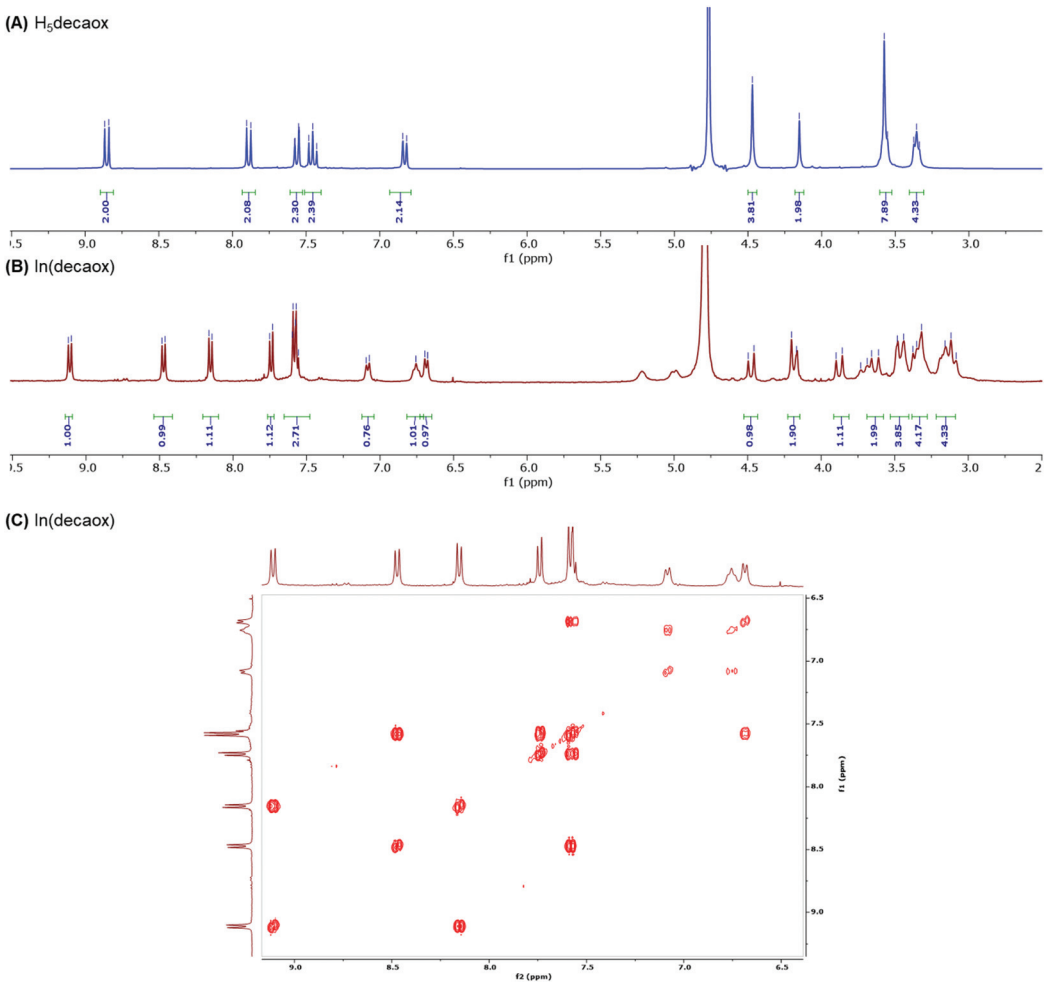

Fig. 2 (A) ^{1}H NMR spectrum (D_2O, RT, 300 MHz) of H_5decaox and (B) ^{1}H NMR spectrum (D_2O, RT, 400 MHz) In(decaox) and (C) partial ^{1}H–^{1}H COSY NMR spectrum (D_2O, RT, 400 MHz) of In(decaox).

opposed to multiple species (Fig. 2B). The complexity of the NMR spectra of the Zr^{4+} and La^{3+} complexes (Fig. S16–S19†) suggests species present with much greater fluxionality and spectral complexity. NMR cannot fully characterise the Zr^{4+} and La^{3+} complexes due to precipitation, as noted with other ligands of high coordination number and DTPA-like backbones, limiting the structural characterization of said complexes in solution.[30,32]

Density functional theory calculations

In the absence of X-ray crystal structures, DFT calculations were undertaken to rationalise the ligand–metal connectivity (Fig. 3). The calculations provide optimised structures showing seven and eight-coordinated Zr^{4+} ions, plus seven-coordinated In^{3+} ions and ten-coordinated La^{3+} ions. Of particular interest are the seven-coordinated In^{3+} ions: the more stable isomer $[In(decaox)]^{2-}$ **B** presents a pentagonal bipyramidal coordination environment (N_3O_4) and has one oxine pendant uncoordinating, consistent with the observations in the ^{1}H NMR solution study (Fig. 3B and S31†). With only one hydroxyquinoline arm coordinated, this structure presents a decreased rigidity and is lower in energy; however, lower kinetic inertness is predicted due to the exceedingly accessible capped carboxylate oxygen in the bipyramidal structure.

For the Zr^{4+} complexes, two minimum energy conformations were found: seven-coordinated (N_2O_5) and eight-coordinated (N_3O_5) Zr^{4+} environments (Fig. 3A and S32†), with only a 12.5 kJ mol^{-1} difference in free energy. The more stable conformation, $[Zr(decaox)]^{-}$ **A**, is the seven coordinated Zr^{4+} ion with a capped octahedral coordination environment. Although only seven-coordinate, isomer **A** is lower in energy, likely due to the shorter bond distances of the bound oxygen to the Zr^{4+} ion (Table S3†).

Two possible conformations were found for the La^{3+} metal complexes, both with N_5O_5 coordination environments saturating the coordination sphere with the decadentate denticity of the ligand (Fig. S33†). Calculations including a coordinated water molecule as seen in the crystal structure of the octadentate chelator H_4octox,[8] showed it was impossible to coordinate any water molecules even with the inclusion of a second

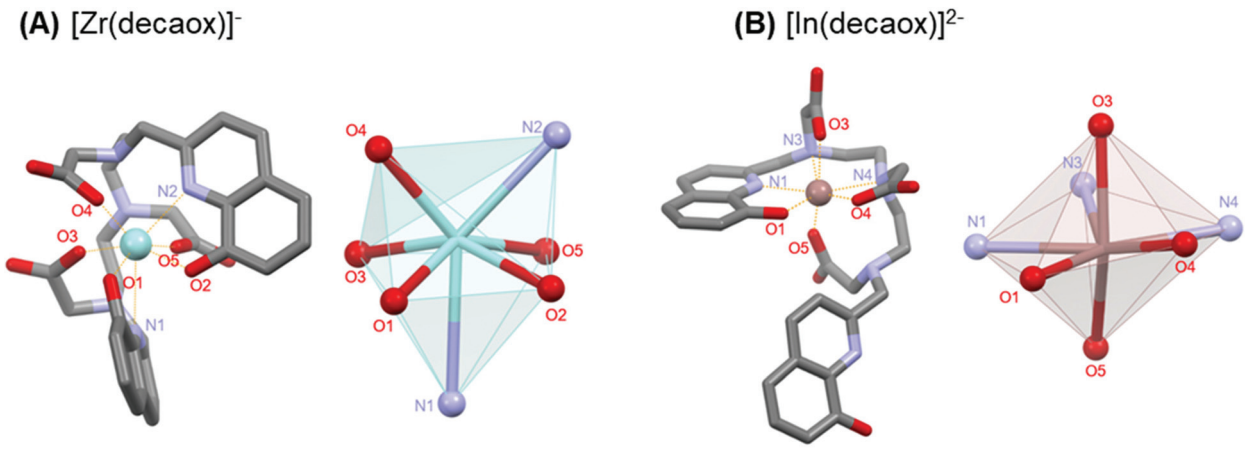

Fig. 3 Optimised structures of the (A) $[Zr(decaox)]^{-}$ **A** and (B) $[In(decaox)]^{2-}$ **B** complex anions obtained with DFT calculations. Bond distances and free energies in Tables S2 and S3.†

sphere of explicit water. It appears that H_5decaox, having shorter overall bond distances of either the three acetate O–M and the two oxine O–M than $[La(octox)]^{-}$, encapsulates La^{3+} better and prevents the coordination of a water molecule.

Solution thermodynamics

To assess the stability of complexes with various metal ions, solution thermodynamic studies can be used to quantify the chelator's ionizable protons and complex formation equilibria. Combined UV-potentiometric titrations were performed to identify the protonation constants and species present over a pH range of 0.2–11.4 of H_5decaox. Analysis of the potentiometric and spectrophotometric data with the HyperQuad,[33] HypSpec2014,[34] and Hyss[35] computer programmes yielded the protonation constants in Table 1, the molar absorptivities of eight absorbing species, and the speciation diagram of H_5decaox (Fig. S24A and S24B†).

As H_5decaox was designed with the oxinate moiety of H_4octox[8] and the diethylenetriamine backbone of H_5decapa,[30] useful comparisons among protonation constants of the three ligands can be made (Table 1). The first protonation constant ($\log K_1$ = 11.0 (1), species HL^{4-}) can be assigned to the central tertiary amine in the backbone and is similar to the $\log K_1$ in H_5decapa. The second and third protonation equilibria ($\log K_2$ = 10.65 (1) and $\log K_3$ = 9.92 (1), species H_2L^{3-} and H_3L^{2-}) involve the protonation of the oxinate oxygens (OH_{ox}) and are consistent with the same functional group protonations in H_4octox. Protonation of the two remaining tertiary amines ($\log K_4$ = 9.12 (1) and $\log K_5$ = 7.32 (1); species H_4L^{-} and H_5L) are in the same order of magnitude as in H_5decapa. The last three protonation equilibria are attributed to the carboxylic acid substituents ($\log K_6$ = 3.64 (1), $\log K_7$ = 2.63 (1) and $\log K_8$ = 1.56 (1)), species H_6L^{+}, H_7L^{2+} and H_8L^{3+}. Protonation of the quinolinium nitrogens was not observed in the experimental conditions but might occur below pH 0.2 (Fig. S23A†).

Complex formation equilibria of H_5decaox with In^{3+}, Zr^{4+} and La^{3+}

Upon determining the protonation constants of the free ligand, similar approaches (titrations and in-batch studies) can be used to assess thermodynamically the stability of the metal–ligand complexes and determine if such complexes will be suitable in physiological applications. This stability is conveyed *via* the formation constant, $\log K$, which represents the thermodynamic driving force for complex formation through the sum of equilibrium equations of each step, expressed as:

Table 1 Protonation constants ($\log K_q$) of discussed ligands

Equilibrium reaction	H_5decaox	H_5decapa[c]	H_4octox[d]
$L + H^+ \leftrightarrows HL$	11.00 (1)[a] ($N_{backbone}$)	11.03 (3) ($N_{backbone}$)	10.65 (1) (OH_{ox})
$HL + H^+ \leftrightarrows H_2L$	10.65 (1)[a] (OH_{ox})	9.20 (3) ($N_{backbone}$)	10.02 (1) (OH_{ox})
$H_2L + H^+ \leftrightarrows H_3L$	9.92 (1)[a] (OH_{ox})	6.86 (4) ($N_{backbone}$)	9.03 (1) ($N_{backbone}$)
$H_3L + H^+ \leftrightarrows H_4L$	9.12 (1)[a] ($N_{backbone}$)	4.43 (4) (py-COOH)	5.18 (1) ($N_{backbone}$)
$H_4L + H^+ \leftrightarrows H_5L$	7.32 (1)[a] ($N_{backbone}$)	3.46 (5) (py-COOH)	3.05 (1) (COOH)
$H_5L + H^+ \leftrightarrows H_6L$	3.64 (1)[a](COOH)	2.84 (6) (COOH)	2.03 (2) (COOH)
$H_6L + H^+ \leftrightarrows H_7L$	2.63 (1)[a] (COOH)	2.52 (4) (COOH)	−0.31 (8) (N_{ox})
$H_7L + H^+ \leftrightarrows H_8L$	1.56 (1)[b] (COOH)	ND	−0.67 (7) (N_{ox})
$\sum \log K \{[H_qL]/[H_{q-1}L][H^+]\}$	**55.80 (1)**	**40.34 (4)**	**38.98 (7)**

[a] Using UV-potentiometric titrations. [b] Using UV batch titration, T = 25 °C, I = 0.16 M NaCl. [c] From ref. 30. [d] From ref. 8. Charges omitted for simplicity.

$pM + qH + rL \leftrightarrow M_pH_qL_r$ (charges omitted for clarity), representing metal ion (M) and ligand (L) association; protons (H^+) here are also important as they compete with metals for occupation of a chelate atom electron pair. Further, the pM value is another way to demonstrate the metal sequestering ability of a ligand in terms of free metal ion concentration under standard conditions (pM = −log([M]) when [L] = 10 μM, [M] = 1 μM, pH 7.4, T = 25 °C).[36] Complex formation equilibria studies of H_5decaox were undertaken with natural stable isotopes of In^{3+}, La^{3+} and Zr^{4+}.

All three metal complexes are mononuclear and present different protonation degrees (species MH_3L, MH_2L, MHL, ML, M(OH)L and additional MH_4L species for La^{3+} – charges omitted for simplicity – Table 2). From the spectroscopic features of the oxine chromophores in these experiments and compared with other well-studied analogous metal complexes with either La^{3+} or In^{3+} and Ga^{3+},[7,8,10,11,37] we can assume that the higher deprotonations of either MH_2L and MHL species correspond to the phenol–OH in the oxine moieties. The most acidic protonations are attributed either to tertiary amines in the backbone or the carboxylic substituents; however, insolubility limited structural elucidation with either NMR or X-ray crystallography.

H_5decaox has a higher affinity for the smaller In^{3+} and Zr^{4+} ions, indicated by the La^{3+} metal complex stability $\log K_{ML}$ being almost half the log value for the corresponding $[Zr(L)]^-$ species (Table 2). The metal complex speciation (M^{n+} = Zr^{4+}, In^{3+} and La^{3+}) was determined with the calculated stability constants (Fig. 4). It is interesting to note that despite the similar $\log K_{ML}$ for the Zr^{4+} and In^{3+} complexes, pZr is 2.4 units higher than is pIn because of the pK_a of the neutral species, Zr(Hdecaox) ($\log K_{MHL}$ = 9.39 (3)) is higher than in $[In(Hdecaox)]^-$ ($\log K_{MHL}$ = 7.53 (2)), translating into less proton competition at pH 7.4. At physiological pH the single species Zr(Hdecaox) predominates, which will be highly advantageous for *in vitro* or *in vivo* assays and medicinal applications. Finally, a comparison of the state-of-art of Zr^{4+} and In^{3+} chelators can be made in terms of pM values (Table 3). While H_5decaox compares amongst the highest pM values for In^{3+} and Zr^{4+} chelating ligands, the kinetic inertness of these metal chelates remains reliable evidence for potential *in vivo* applications and these promising thermodynamic stability results are essential for further *in vitro*/*in vivo* studies.

Table 2 Stability constants ($\log K_{ML}$) and corresponding stepwise protonation constants $\log K_{1q1}(MH_qL)$[a] of H_5decaox with In^{3+}, La^{3+} and Zr^{4+} (T = 25 °C, I = 0.16 M NaCl)

	Zr^{4+}	In^{3+}	La^{3+}
$\log K_{101}$ (ML)	43.06 (3)	42.32 (2)	24.6 (2)
$\log K_{111}$ (MHL)	9.39 (3)	7.53 (2)	9.17 (1)
$\log K_{121}$ (MH_2L)	5.13 (2)	5.02 (3)	7.84 (1)
$\log K_{131}$ (MH_3L)	3.53 (2)	2.40 (1)	5.12 (2)
$\log K_{141}$ (MH_4L)	—	—	3.64 (2)
$\log K_{1-11}$ (M(OH)L)	9.44 (3)	10.51 (3)	10.66 (2)
pM	**34.7**	**32.3**	**16.5**

[a] $K_{1q1} = [MH_qL]/[MH_{q-1}L][H]^q$; $(q-1) = -1$ denotes OH.

Radiolabeling and serum stability

Based on the nonradioactive metal complexation, solution studies and available isotopes, radiolabeling with both $[^{111}In]InCl_3$ and $[^{89}Zr]ZrCl_4$ proceeded in a concentration dependent manner. Since the attempted radio-TLC plates and conditions gave inconsistent results for $[^{111}In]InCl_3$ radiolabeling, radio-HPLC was used to determine the radiochemical yield during concentration dependent studies with both $[^{111}In]InCl_3$ and $[^{89}Zr]ZrCl_4$ (Fig. 5 and Table S1†). With $[^{111}In]InCl_3$ (3 MBq per reaction), radiolabeling was quantitative with ligand concentrations 100, 10 and 1 μM and 89% at 0.1 μM in NaOAc buffer (0.1 M, pH 7) at room temperature for 30 minutes. Radiolabeling with $[^{89}Zr]ZrCl_4$ (2 MBq per reaction) under the same conditions (NaOAc buffer, 30 min, RT) showed similar results for 100 and 10 μM, but RCY dropped off to 89% at 1 μM. Additionally, the distribution coefficient of the $[^{89}Zr]Zr$ (decaox) complex at pH 7.4 was investigated using a two-phase extraction system from 1-octanol/aqueous buffer to understand the hydrophilic nature of the complex. The $\log D_{7.4}$ was determined to be −0.822 ± 0.004, a reasonably hydrophilic complex comparable to the recently reported DFO2 (−0.71) although more lipophilic than DFO itself (−2.70).[42] Finally, radiolabel-

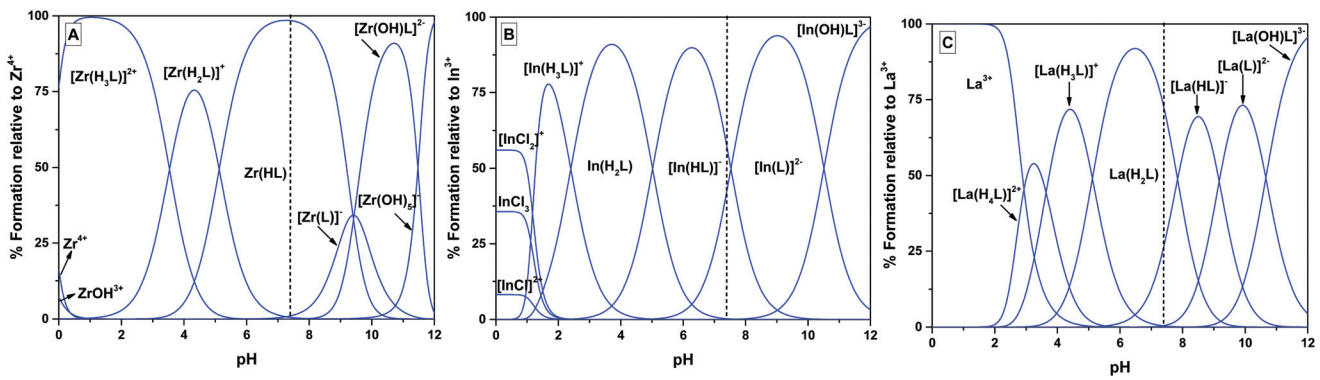

Fig. 4 Speciation plots of H_5decaox metal complexes: (A) Zr^{4+}, (B) In^{3+}, and (C) La^{3+} ; dashed line indicates pH 7.4.

Table 3 pM[a] values of selected chelating ligands (Mn^{+} = In^{3+}, Zr^{4+})

	pIn		pZr
H_5decaox	**32.3**[b]	H_5decaox	**34.7**[b]
8-Hydroxyquinoline	34.1[30]	DFO	32.2[38]
DTPA	25.7[30]	DTPA	33.9[38]
H_4octox	25.0[8]	3,4,3-LI(1,2-HOPO)	44.0[39]
H_3glyox	34[10]	THPN	42.8[40]
H_4pypa	30.5[41]	AHA	28.9[38]
H_4octapa	26.5[30]		
DOTA	18.8[30]		

[a] pM = $-\log[\text{Metal}]_{free}$, [L] = 10 μM, [M] = 1 μM, pH = 7.4.[36] [b] This work.

Table 4 Serum stability of selected chelators with $[^{111}In]In^{3+}$

Complex	1 h stability (%)	24 h stability (%)	5 day stability (%)
$[^{111}In][In(decaox)]^{2-}$	97.3 ± 0.4	91 ± 1	63 ± 6
$[^{111}In][In(octox)]^{-}$ [a]	96.2 ± 0.4	91.4 ± 0.6	83.6 ± 1.4
$[^{111}In][In(decapa)]^{2-}$ [b]	89.7 ± 1.6	89.1 ± 1.7	ND
$[^{111}In][In(octapa)]^{-}$ [b]	93.8 ± 3.6	92.3 ± 0.04	ND
$[^{111}In][In(DOTA)]^{-}$ [b]	89.6 ± 2.1	89.4 ± 2.2	ND
$[^{111}In][In(DTPA)]^{2-}$ [b]	86.5 ± 2.2	88.43 ± 2.2	ND

[a] From ref. 8. [b] From ref. 30.

ing with the larger, therapeutic radiometal ion, $[^{225}Ac]Ac^{3+}$ was unsuccessful in varying conditions: 0.1 M or 1 M NaOAc, pH 7, RT and 80 °C. This corroborates with the solution studies with La^{3+} (cold metal surrogate of $^{225}Ac^{3+}$) that suggested weak thermodynamic stability of the $[La(decaox)]^{2-}$ complex, especially in comparison to the In^{3+} and Zr^{4+} complexes.

Following successful radiolabeling with both $[^{111}In]InCl_3$ and $[^{89}Zr]ZrCl_4$, the kinetic inertness of the resulting complexes towards human serum proteins was investigated in a protein challenge experiment using either PD-10 size exclusion desalting columns[43] with $[^{111}In]In(decaox)$ complex, and protein precipitation with cold acetonitrile[42] for the $[^{89}Zr]Zr$(decaox) complex. Many endogenous proteins found in human serum, such as *apo*-transferrin and albumin, are capable of competing for metal ion binding, and a successful radiometal–ligand complex must withstand transchelation towards such proteins. For the $[^{111}In]In(decaox)$ complex, within 24 hours a slight decrease to 91% intact was observed, which continued to slowly decomplex to only 63% intact complex at the final five-day time point (Fig. 5B). This 24-hour decrease is similar to previously reported ligands following the same methodology, including $[^{111}In][In(decapa)]^{2-}$, $[^{111}In][In(DOTA)]^{-}$ and $[^{111}In][In(DTPA)]^{2-}$ (Table 4). However, the five-day stability is only compared to that of $[In(octox)]^{-}$, which indicates the smaller oxinate ligand H_4octox may be better suited for $[^{111}In]In^{3+}$ (Table 4). The DFT calculated structure indicating decreased rigidity with only one hydroxyquinoline bound and labile points from the lack of encapsulation near the carboxylic acid provides an explanation of the susceptible $[^{111}In]In^{3+}$ ion towards serum proteins.

After 24 hours $[^{89}Zr]Zr$(decaox) remained 86% intact, indicating the initial decomplexation is common in both complexes. Over 7 days, $[^{89}Zr]Zr$(decaox) remained 75% intact, indicating a higher stability than for $[^{111}In]In$(decaox), and slightly less stable when compared to DFO and DFO-type ligands using the same method (Table 5).[42] Interestingly, the $[^{89}Zr]Zr$(decaox) complex is significantly more stable than is $[^{89}Zr]Zr$(decapa),[44] which incorporates picolinic acid moieties in lieu of the oxinates found in H_5decaox. This indicates that the rigidity of the bicyclic oxine groups has had the desired improved stability in this case compared to picolinic acid ligands. The observed decrease in stability in both $[^{111}In][In(decaox)]^{2-}$ and $[^{89}Zr][Zr$

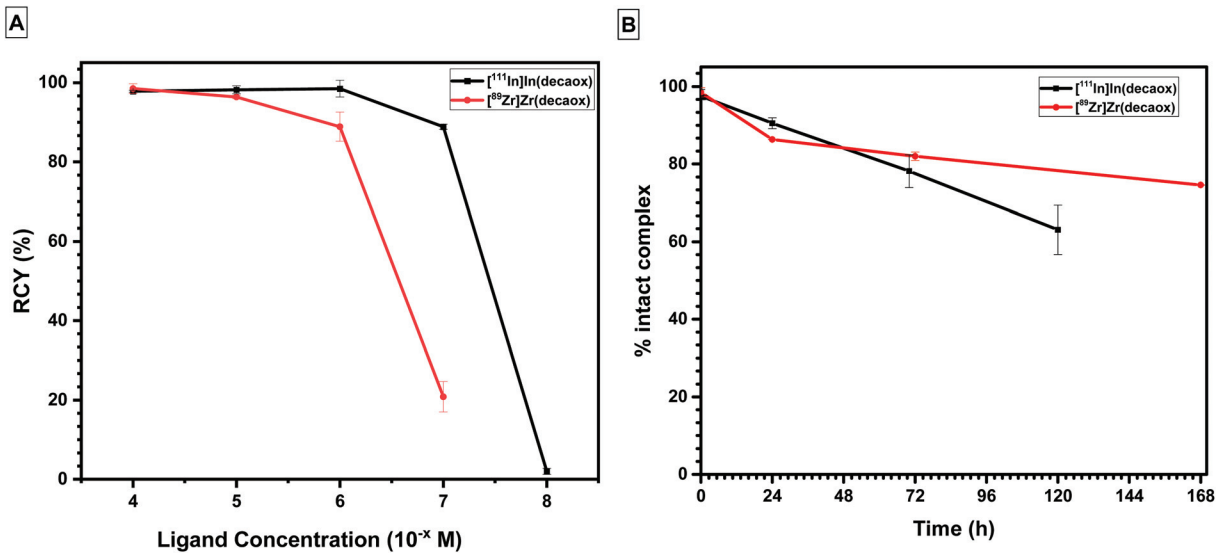

Fig. 5 (A) Concentration dependent radiolabeling of H_5decaox with $[^{111}In]In^{3+}$ (black) and $[^{89}Zr]Zr^{4+}$ (red) in NaOAc (0.1 M, pH 7), 30 min, RT, n = 2, monitored by radio-HPLC. (B) Serum stability of $[^{111}In]In$(decaox) and $[^{89}Zr]Zr$(decaox), n = 3.

Table 5 Serum stability of selected chelators with $[^{89}Zr]Zr^{4+}$

Complex	1 day stability (%)	3 day stability (%)	7 day stability (%)
$[^{89}Zr][Zr(decaox)]^-$	86.3 ± 0.1	86 ± 1	74.6 ± 0.1
$[^{89}Zr][Zr(decapa)]^-$ [a]	~26	~17	ND
$[^{89}Zr][Zr(DFO2)]^-$ [b]	~93	~96	87 ± 1
$[^{89}Zr][Zr(DFO)]^-$ [b]	~80	~83	81 ± 4

[a] From ref. 44. [b] From ref. 42.

(decaox)]$^-$ may also be due to non-specific protein interactions rather than decomplexation, considering the hydrophobic nature of the complexes; this has been reported with several, similar lipophilic M–oxine complexes.[45–47] Further, *in vitro* serum stability assessments are not always predictive the *in vivo* behaviour of metal–ligand complexes, and overall, the mild and rapid radiolabeling conditions while remaining comparably stable over 24 hours suggest the promise of the H_5decaox new chelating ligand radiopharmaceutical development.

Conclusions and outlook

A new potentially decadentate, oxine-containing ligand was synthesised from the diethylenetriamine backbone. This ligand has been assessed by both radioactive and non-radioactive metal complexation studies with various metal ions ($[^{nat/111}In]In^{3+}$; $[^{nat/89}Zr]Zr^{4+}$; $^{nat}La^{3+}$/$[^{225}Ac]Ac^{3+}$). The increased denticity and cavity size of the ligand compared to previously reported 'ox' ligands can accommodate larger metal ions or different charged ions, as indicated in the high thermodynamic stability constants with In^{3+} and Zr^{4+}. Mild radiolabeling conditions led to high radiochemical yields at micromolar concentrations with both $[^{111}In]InCl_3$ and $[^{89}Zr]ZrCl_4$ and the intact complex after 24 hours in the presence of serum proteins indicates H_5decaox as a promising chelate for radiometal isotopes. DFT calculations complement the solution thermodynamics and serum stability, evinced in the seven-coordinate complexes with Zr^{4+} and In^{3+}, having N_2O_5 and N_3O_4 atom environments, respectively. H_5decaox appears to be extremely well-suited for the harder metal ion Zr^{4+}, with shorter Zr–O bond lengths, and a better match for the hard donor hydroxyquinoline units. Further, the central carboxylic acid moiety presents an interesting accessible position for functionalization to imbue a targeted, bifunctional chelator with similar capabilities; synthesis and characterisation of a functionalised version of this highly promising ligand is underway and will be assessed as a bioconjugate.

Experimental section

Materials and methods

All reagents and solvents were purchased from commercial suppliers (Sigma-Aldrich, AKScientific, TCI) and used as received unless otherwise indicated. Aluminum-backed ultrapure silica gel 60 Å, 250 μm thickness analytical TLC plates were used for reaction monitoring. Flash column chromatography was performed using silica gel sourced from Silicycle (Siliaflash irregular silica gels F60, 60 Å pore size, 40–63 mm particle size). Automated purification was performed using a Teledyne Isco CombiFlash R_f automated system, using RediSep R_f Gold normal-phase silica, neutral alumina, and reverse-phase C18 re-useable column cartridges. ^1H, $^{13}C\{^1H\}$ and COSY NMR spectra were measured on Bruker AV300 and AV400 spectrometers at ambient temperature unless otherwise stated and interpreted using Mestrenova spectral visualization software. Low-resolution mass spectrometry was carried out using a Waters liquid-chromatography – mass-spectrometer system consisting of a Waters ZQ quadrupole spectrometer coupled to an ESCI ion source and a Waters 2695 HPLC system. HRMS was performed on a Waters Micromass LCT – TOF instrument at the University of British Columbia. Microanalyses for C, H, and N were performed on a Carlo Erba elemental analyzer EA 1108. $[^{111}In]InCl_3$ was produced and purchased from BWX Technologies as a 0.05 M HCl solution. $[^{225}Ac]Ac^{3+}$ was provided by Canadian Nuclear Laboratories (CNL) from decay of ^{229}Th and separation from ^{233}U. Upon arrival, $[^{225}Ac]Ac^{3+}$ was purified by branched DGA resin column to remove chemical impurities and re-constituted in 0.01 M HNO_3. $[^{89}Zr]Zr^{4+}$ was produced from the $[^{89}Y(p,n)^{89}Zr]$ reaction at either HZDR or University of Alabama Birmingham as $[^{89}Zr]ZrCl_4$ or $[^{89}Zr]Zr$ (oxalate), respectively. Radiolabeling progression was monitored using radioHPLC with a Knauer Smartline System consisting of Smartline 1000 pump, K2501 UV detector, Raytest Gabi Star activity detector, Chromgate 2.8 software and a Smartline 5000 manager with a Phenomenex Synergi 4-micron Hydro/HP 80 A 250 × 4.6 mm or an Agilent 1260 Infinity II Quaternary Pump, Agilent 1260 Autosampler, Raytest Gabi Star NaI(Tl) radiation detector, Agilent 1260 variable wavelength detector, with a Phenomenex Luna C18 analytical column (4.6 × 250 mm, 5 μm).

Synthesis and characterisation

8-Hydroxy-2-carbaldehyde (1). Compound **1** was prepared according to the literature with appropriate characterisation and spectra.[7,16]

2-(Hydroxymethyl)quinolin-8-ol (2). Compound **1** (499 mg, 2.88 mmol) was dissolved in MeOH (20 mL) and cooled to 0 °C in an ice-water bath. $NaBH_4$ (220 mg, 5.76 mmol) was added to the stirring solution, which was subsequently warmed to RT and stirred overnight. The reaction mixture was quenched with H_2O (20 mL), acidified with 1 M HCl (5 mL) and extracted with CH_2Cl_2 (3 × 25 mL). The organic phases were combined and dried over Na_2SO_4 and evaporated to give an off white solid (381 mg, 75%). ^1H NMR ($CDCl_3$, 400 MHz) δ 8.19 (d, 1H, J = 8.5 Hz), 7.48 (t, 1H, J = 7.9 Hz), 7.40 (m, 2H, J = 8.5 Hz), 7.25 (d, 1H, J = 7.6 Hz), 5.00 (s, 2H). $^{13}C\{^1H\}$ NMR ($CDCl_3$, 75 MHz) δ 137.3, 127.6, 119.4, 118.2, 111.1, 64.9. LR-ESI-MS: calcd for $[C_{10}H_9NO_2]$: 175.1; found: $[M + H]^+$: 176.3

2-(Bromomethyl)quinoline-8-ol (3). Compound **2** (217 mg, 1.24 mmol) was dissolved in dry CH_2Cl_2 (12 mL) and cooled to 0 °C in an ice-water bath. PBr_3 (128 μL, 1.36 mmol) dissolved in dry CH_2Cl_2 (1 mL) was added dropwise to the solution with stirring. The reaction mixture was stirred at 0 °C for 5 h before sat. $NaHCO_3$ (20 mL) was added to quench. The reaction mixture was extracted with CH_2Cl_2 (3 × 25 mL), and the combined organic phases were dried over Na_2SO_4 and evaporated to give the title compound as a light-yellow residue (218 mg, 74%). ^{1}H NMR ($CDCl_3$, 400 MHz) δ 8.19 (d, 1H, J = 8.5 Hz), 7.61 (d, 1H, J = 8.5 Hz), 7.49 (t, 1H, J = 7.8 Hz), 7.35 (d, 1H, J = 8.2 Hz), 7.22 (d, 1H, J = 8.6 Hz), 4.73 (s, 2H). ^{13}C{^{1}H} NMR ($CDCl_3$, 75 MHz) δ 137.5, 128.4, 122.0, 117.8, 110.8, 33.9. LR-ESI-MS: calcd for [$C_{10}H_8BrNO$]: 236.98; found [M(^{79}Br) + H]$^+$: 238.1, and [M(^{81}Br) + H]$^+$: 240.2.

***N,N′*-(2-Nitrobenzensulfonamide)-1,2-triaminodiethane (4).** Diethylenetriamine (1.5 mL, 15.2 mmol) was dissolved in dry THF (90 mL) and cooled to 0 °C. Na_2CO_3 (3.21 g, 30.4 mmol) was added to the stirring solution, followed by the slow addition of 2-nitrobenzene sulfonyl chloride (6.75 g, 30.4 mmol). Upon complete addition of the reagents, the solution was warmed to RT and stirred overnight. The salts were removed by filtration and the solvent evaporated *in vacuo* to give a yellow solid, which was recrystallized in DCM to give an off-white solid (3.2 g, 52%). ^{1}H NMR (CD_3CN, 400 MHz) δ 8.03 (m, 2H), 7.85 (m, 2H), 7.80 (m, 4H), 2.99 (t, 4H, J = 5.7, 6.2 Hz), 2.54 (t, 4H, J = 5.6, 6.2 Hz). ^{13}C{^{1}H} NMR (CD_3CN, 100 MHz) δ 134.1, 132.9, 132.7, 130.6, 125.1, 47.2, 42.9. LR-ESI-MS: calcd for [$C_{16}H_{19}N_5O_8S_2$]: 473.07; found [M + H]$^+$: 473.9.

Di-*tert*-butyl2,2′-((((2-(tert-butoxy)-2-oxo ethyl) aza nediyl) bis (ethane-2,1-diyl)) bis ((phenylsulfonyl) aza nediyl))diacetate (5). K_2CO_3 (2.15 g, 15.5 mmol) was added to a stirring solution of compound **4** (1.05 g, 2.22 mmol) in dry CH_3CN (20 mL). To this solution was added *tert*-butyl bromoacetate (1.08 mL, 7.32 mmol) and the mixture was heated at 60 °C for 24 h. The salts were filtered from the reaction mixture and the solvents were evaporated *in vacuo*. The resulting residue was re-dissolved in H_2O (30 mL) and extracted with EtOAc (3 × 50 mL). The combined organic layers were washed once with sat. $NaHCO_3$ (25 mL) and water (25 mL) and dried over $MgSO_4$. The solvents were evaporated *in vacuo* to give a yellow oil (1.74 g, 96%). ^{1}H NMR ($CDCl_3$, 400 MHz) δ 8.05 (m, 2H), 7.66 (m, 4H), 7.55 (m, 2H), 4.14 (s, 4H), 3.44 (t, 4H, J = 6.9 Hz), 3.22 (s, 2H), 2.85 (t, 4H, J = 6.9 Hz), 1.42 (s, 9H), 1.32 (s, 18H). ^{13}C{^{1}H} NMR ($CDCl_3$, 100 MHz) δ 167.8, 147.9, 133.5, 131.8, 130.9, 123.9, 82.3, 60.4, 53.2, 49.5, 46.7, 28.1, 27.9, 21.1, 14.2. LR-ESI-MS: calcd for [$C_{34}H_{49}N_5O_{14}S_2$]: 815.27; found [M + H]$^+$: 816.5.

Di-*tert*-butyl 2,2′-((((2-(tert-butoxy)-2-oxo ethyl) aza nediyl) bis (ethane-2,1-diyl)) bis (aza nediyl))-diacetate (6). Compound **5** (1.40 g, 1.72 mmol) was dissolved in dry CH_3CN (20 mL) and the flask purged with nitrogen. Thiophenol (440 μL, 4.31 mmol) was added to the stirring solution followed by K_2CO_3 (816 mg, 5.70 mmol). The reaction mixture was heated at 60 °C and stirred for 24 h, before cooling to RT and removing salts *via* centrifugation. The residue was re-dissolved in water (50 mL) and extracted with EtOAc (3 × 50 mL). The organic phases were combined, washed with sat. $NaHCO_3$ (30 mL), dried over $MgSO_4$ and the solvents evaporated *in vacuo*. The crude material was purified *via* flash column (Al_2O_3) chromatography (Combiflash automated purification system, A: Hexanes, B: EtOAc; 100% A to 20% B) to give a yellow oil (432 mg, 56%). ^{1}H NMR ($CDCl_3$, 100 MHz) δ 3.33 (s, 2H), 3.31 (s, 4H), 2.80 (t, 4H, J = 6.0 Hz), 2.66 (t, 4H, J = 6.0 Hz), 1.45 (s, 18 H), 1.44 (s, 9H). ^{13}C{^{1}H} NMR ($CDCl_3$, 100 MHz) δ 171.6, 171.0, 81.1, 80.9, 55.8, 54.1, 51.6, 47.3, 28.3, 28.2. LR-ESI-MS: calcd for [$C_{22}H_{43}N_3O_6$]: 445.32; found [M + H]$^+$: 446.3.

H_5decaox (7). Compound **6** (101 mg, 0.23 mmol) was dissolved in dry CH_3CN and the flask purged with N_2. K_2CO_3 (130 mg, 0.94 mmol) was added to the solution. Compound **3** (130 mg, 0.53 mmol) was dissolved in dry CH_3CN and added to the stirring reaction mixture. The reaction mixture was heated to 60 °C and stirred overnight, after which time it turned a deep brown colour. The reaction mixture was removed from heat and cooled to room temperature before salts were filtered out. The collected filtrate was evaporated, dissolved in H_2O and the pH was adjusted to 5 before extracting with EtOAc (3 × 15 mL). The combined organic layers were dried over Na_2SO_4, filtered and evaporated to give a brown residue that was used without purification in the next deprotection step. The brown residue was dissolved in THF (2 mL) and 6 M HCl (2 mL) was added. The reaction mixture was heated to 40 °C and stirred for 18 h before evaporating the solvents for purification. The crude product was purified by reverse phase C18 column chromatography (Combiflash automated purification system, A: H_2O + 0.01% TFA, B: CH_3CN; 95% A to 45% A). Combined fractions yielded the product H_5decaox as a yellow residue (76 mg, 30% over two steps). ^{1}H NMR (D_2O, 300 MHz) δ 8.85 (d, 2H, J = 8.5 Hz), 7.89 (d, 2H, J = 8.6 Hz), 7.56 (d, 2H, J = 7.9), 7.46 (t, 2H, J = 16.0, 7.9), 6.83 (d, 2H, J = 7.7), 4.47 (s, 4H), 4.15 (s, 2H), 3.58 (s, 8H), 3.37 (t, 4H, J = 11.6, 5.8). ^{13}C{^{1}H} NMR (D_2O, 75 MHz) δ 175.8, 169.7, 154.3, 147.4, 146.5, 130.7, 129.3, 129.2, 122.5, 119.6, 116.8, 56.3, 54.9, 54.6, 51.1. LR-ESI-MS calcd for [$C_{30}H_{33}N_5O_8$] 591.23; [M + H]$^+$: 592.3. HR-ESI-MS calcd for [$C_{30}H_{33}N_5O_8$ + H]: 592.2407; found [M + H]$^+$: 591.2401. Elemental Analysis calc'd % for H_5decaox·5HCl·2.8H_2O ($C_{30}H_{33}N_5O_8$·5HCl·2.8H_2O): C 43.71, H 5.33, N 8.50. Found: C 43.93, H 5.52, N 8.26.

Metal complexation

A stock solution of H_5decaox (10 mM) was prepared in D_2O for metal complex NMR characterisation. Metal ions of interest (M = In^{3+}, La^{3+}, Zr^{4+}) were similarly prepared as stock solutions in D_2O (10 mM) and complexes were prepared by combining 1 : 1.1/L : M (V_t ~400 μL) and adjusting the pH with freshly prepared 0.1 M NaOD. Solutions stood at RT for at least 15 minutes prior to collecting NMR spectra.

Na[In(Hdecaox)]. HR-ESI-MS calcd for $C_{30}H_{30}InNaN_5O_8$ 726.1031; measured 726.1027.

[Zr(Hdecaox)]. HR-ESI-MS calcd for $C_{30}H_{30}N_5O_8Zr$ 678.1141; measured 678.1144.

[La(H$_2$decaox)]. HR-ESI-MS calcd for $C_{30}H_{31}{}^{139}LaN_5O_8$ 728.1236; measured 728.1234.

Radiolabeling and serum stability assays

[^{111}In]In^{3+} radiolabeling. A stock solution of H$_5$decaox (1×10^{-3} M) was prepared in H_2O and used in serial dilutions for concentration dependent radiolabeling experiments. Radiolabeling reactions were prepared to a total volume of 500 μL in NaOAc buffer (0.1 M, pH 7), with ligand concentrations of 1×10^{-4} to 10^{-8} M, upon which 1 μL (~3 MBq) of [^{111}In]InCl$_3$ was added and incubated at RT for 30 minutes. Reaction progress was monitored by radio-HPLC using a linear gradient of 5%–60% A (A = CH_3CN, B = H_2O + 0.1% TFA) over 20 minutes, where free [^{111}In]InCl$_3$ elutes at R_t = 4.8 min and radiolabeled complex elutes at R_t = 11.6 min. The area of each peak was integrated and used to determine RCY%.

Serum stability of the [^{111}In]In(decaox) complex was evaluated using GE Healthcare Life Sciences PD-10 desalting column (size exclusion <5000 Da) method as previously described.[43] In triplicate, a quantitatively labeled reaction ([L] = 1×10^{-5} M) with ~37 MBq (1 mCi) of activity was combined with an equal volume (500 μL) of human serum and incubated at 37 °C. At time points of 1 h, 1 day, 3 days and 5 days, aliquots of 100, 200, 200 and 400 μL respectively, were diluted to 2.5 mL and the activity was measured with a CRC55tR dose calibrator. The dilution was then loaded onto an equilibrated PD-10 desalting column, and the activity of the empty vial was measured to determine the "residual activity". Upon column adsorption, the proteins (MW >5000 Da) were eluted with 3.5 mL of PBS. The activity of the elution was then measured, and the stability of the complex in % was calculated as in eqn (1).

$$\%\ \text{stability} = 1 - \left(\frac{(\text{Activity of elution})}{(\text{Activity of load}) - (\text{Activity residual})}\right) \quad (1)$$

[^{89}Zr]Zr^{4+} radiolabeling. A stock solution of H$_5$decaox (1×10^{-3} M) was prepared in H_2O and diluted further for concentration dependent experiments. Radiolabeling reactions took place in a total reaction volume of 200 μL, at ligand concentrations of 1×10^{-4} to 10^{-7} M in NaOAc buffer (0.1 M, pH 7) and ~2 MBq of [^{89}Zr]ZrCl$_4$. The reaction progress was monitored at 30 minutes using radio-HPLC on a C18 column with solvents A (H_2O + 0.1% TFA) and B (CH_3CN + 0.1% TFA) in a gradient of 100% A to 100% B over 20 minutes, where free [^{89}Zr]ZrCl$_4$ elutes at R_t = 3.30 min and complexed [^{89}Zr]Zr (decaox) elutes at R_t = 8.8 min. The area of each peak was integrated and used to determine RCY%.

The serum stability of a quantitatively radiolabeled sample of [^{89}Zr]Zr(decaox) was determined using a protein precipitation method with cold CH_3CN following literature precedents.[42] In triplicate, 400 μL of a quantitatively radiolabeled sample of [^{89}Zr]Zr(decaox) (~4 MBq, [L] = 1×10^{-4} M) was added to a vial with 600 μL of human serum and incubated at 37 °C over a 7 day period. The stability of the complex to transchelation was analyzed on day 1, 3, and 7 by adding 300 μL aliquots to ice cold CH_3CN (700 μL) to precipitate the serum proteins. This sample was centrifuged for 10 min at 10 000 rpm, and the supernatant was decanted and counted in a dose calibrator. A second wash of H_2O/CH_3CN (30 : 70) was added to the pellet, and re-centrifuged for another 10 min at 10 000 rpm. The supernatant was decanted and counted in a dose calibrator. The amount of [^{89}Zr]Zr^{4+} that remained within the centrifuged pellet was assumed to be transchelated, while the amount of [^{89}Zr]Zr^{4+} in the combined supernatant was assumed to be intact complex, and this ratio was used to determine the percent stability.

The distribution coefficient (log D) was determined at pH 7.4, performed in duplicate and each duplicate measured twice. A stock solution of $ZrCl_4$ (1×10^{-4}) and [^{89}Zr]ZrCl$_4$ (4 MBq) was prepared and 50 μL was added to a solution of H$_5$decaox (1×10^{-4} M) to a total reaction volume of 500 μL in NaOAc buffer (0.1 M, pH 7). Quantitative radiolabeling was confirmed by HPLC, and 50 μL of the reaction mixture was added to a mixture of octanol (500 μL) and HEPES buffer/NaOH (450 μL, pH 7.4). These samples were mixed for 30 minutes at RT and then allowed to separate. 400 μL from each octanol and water phase was removed and centrifuged. Duplicates of each sample (100 μL) from each sample were then counted in a gamma counter (NaI(Tl) scintillation counter automatic gamma counter 1480, Wizard 3″, PerkinElmer) and used to determine the octanol/water distribution ratio of [^{89}Zr]Zr(decaox) following eqn (2).

$$\log D_{7.4} = \log_{10}\left(\frac{\text{Counts in octanol phase}}{\text{Counts in aqueous phase}}\right) \quad (2)$$

Solution thermodynamics

Protonation constants and metal stability constants were determined from a combined UV-potentiometric titration system using a Metrohm Titrando 809 equipped with a Ross combined electrode, a Metrohm Dosino 800, and a Varian Cary 60 UV/vis spectrophotometer (200–500 nm spectral range) connected to a 0.2 cm path length optic dip probe submerged in the titration cell. The titration cell consisted of a 20 mL thermostatted glass cell at 25 °C with an inlet–outlet tube for nitrogen gas to exclude any CO_2 before and throughout the titration. The electrode was calibrated daily for hydrogen ion concentration using a standard HCl and calibration data were analysed with the Gran procedure[48] to obtain calibration parameters E^0 and pK_w. Solutions were titrated with carbonate-free NaOH (0.16 M) that was standardised against freshly recrystallised potassium hydrogen phthalate. Protonation equilibria of the ligand were studied *via* combined UV-potentiometric titrations of a solution containing H$_5$decaox ([L] = 9.62×10^{-4} M, 25 °C, l = 0.2 cm and 0.16 M NaCl). Electromotive force values and spectra were recorded after each NaOH addition, and the apparatuses were synchronized to have constant delays between each titrant addition and sufficient time to reach equilibrium.[33] The dissociation of the most acidic protons

were evaluated *via* in batch UV-spectrophotometric samples ([L] = 2.25×10^{-5} M) measured and recorded in a 1 cm path length cuvette, as the pH was below the electrode threshold.

Complex formation equilibria with In^{3+} or La^{3+} and H_5decaox were directly studied *via* UV-potentiometric titrations. Ligand–metal solutions were prepared by adding the atomic absorption (AA) standard metal ions solutions to a known concentration of H_5decaox (([L] = [In^{3+}] = 7.67×10^{-4} M) and ([L] = [La^{3+}] = 8.31×10^{-4} M)) at 25 °C and ionic strength of 0.16 M NaCl. For highly acidic dissociation constants with In^{3+} ([L] = [In^{3+}] = 2.25×10^{-5} M) and all samples with Zr^{4+} ([L] = [Zr^{4+}] = 2.0×10^{-5} M), in batch samples were prepared and UV-spectrophotometry was measured individually in a 1 cm path length cuvette. All potentiometric measurements were processed using Hyperquad2013 software,[33] while the obtained spectrophotometric data were processed with the HypSpec2014 program.[34] Molar absorptivities of protonated species of H_5decaox were included in metal stability calculations, and proton dissociation constants corresponding to the hydrolysis of In^{3+} and La^{3+} aqueous ions were taken from Baes and Mesmer.[49,50] By convention, a complex containing a metal ion, M, proton, H, and ligand, L, has the general formula $M_pH_qL_r$ and the overall equilibrium formation constant is designated $\log\beta$ and is characterized by the general equilibrium: $pM + qH + rL = M_pH_qL_r$ (charges omitted). The stoichiometric indices p might also be 0 in the case of protonation equilibria, and negative values of q refer to proton removal from metal-ion-coordinated water, equivalent to hydroxide ion addition to the complex. Stepwise equilibrium constants, $\log K$, correspond to the difference in log units between the overall constants of sequentially protonated (or hydroxide) species. pM is defined as ($-\log[M^{n+}]_{free}$) and was calculated using the Hyss software[35] from the stability constants for each system using the standards: [M^{n+}] = 1 μM, [L^{x-}] = 10 μM, pH 7.4, and 25 °C.[36]

Density functional theory calculations

All DFT calculations were performed using Gaussian 16 revision c01.[51] Self-consistent field (SCF) convergence criteria were set to their default values (SCF = Tight in Gaussian). Structure optimisations were performed without symmetry constraints using the Berny algorithm[52] with default settings, starting from initial structures built manually. Each structure was optimised and free energies were calculated using DFT with the PBE0 hybrid exchange–correlation functional,[53] added D3 (BJ)[54–56] dispersion corrections, and the def2-TZVP basis set[57] for all non-metal atoms. Effective core potentials (ECPs) were used to account for scalar relativistic effects in metal core electrons. Specifically, def2-TZVP basis sets were used with ECPs for zirconium[58] and for indium[57,59] while the Stuttgart RSC segmented valence basis set and ECP[60,61] was used for lanthanum. Metal basis sets were downloaded from the Basis Set Exchange website.[62–64] The PBE0 functional was chosen due to its previous success in structure prediction and thermochemistry of transition metal complexes,[65–69] while the def2-TZVP basis was chosen as a reasonable trade-off between speed and accuracy for the large system sizes under study.[70,71] The integral equation formalism of the polarizable continuum model (IEFPCM) was used as an implicit water model in all calculations to simulate the average dielectric effects of the solvent. Default IEFPCM parameters were used, as implemented in Gaussian (ε = 78.36, van der Waals surface without "added spheres"). Each calculation was repeated with 0 and 4 explicit water molecules which were placed randomly by the PACKMOL code[72] in a sphere up to 4.5 Å from each system's centre of mass. Adjustments were then made before optimisation to move the randomly placed water molecules closer to hydrogen bond centers, such as hydroxyquinolinate and carboxyl groups. Calculation results were visualized using GaussView version 6.0[73] and Avogadro version 1.2.0.[74]

Conflicts of interest

The authors declare no competing financial interest.

Acknowledgements

We gratefully acknowledge the Natural Sciences and Engineering Research Council (NSERC) of Canada for CGS-M/PGS-D scholarships (L. S.), UBC for a Four Year Fellowship (L. S.) and the NSERC CREATE IsoSiM program at TRIUMF for research stipends (L. S., L. W.). We thank both NSERC and CIHR for financial support *via* a Collaborative Health Research Project (CHRP – CO) and NSERC Discovery (CO). We thank WestGrid and Compute Canada for access to their computational resources. We gratefully acknowledge Dr Maria Ezhova for her expert advice on NMR experiments, Karin Landrock for technical assistance at HZDR, Dr Martin Walther for providing ^{89}Zr at HZDR and Hayden Scheiber for helpful DFT discussions. We heartily thank Randy Perron and Dr Patrick Causey at CNL for providing the ^{225}Ac. HZDR is thanked for supporting the IsoSiM International Research Experience program; TRIUMF receives federal funding *via* a contribution agreement with the National Research Council of Canada.

References

1 M. D. Bartholomä, *Inorg. Chim. Acta*, 2012, **389**, 36–51.
2 D. Brasse and A. Nonat, *Dalton Trans.*, 2015, **44**, 4845–4858.
3 E. Boros and A. B. Packard, *Chem. Rev.*, 2019, **119**, 870–901.
4 T. I. Kostelnik and C. Orvig, *Chem. Rev.*, 2019, **119**, 902–956.
5 C. F. Ramogida and C. Orvig, *Chem. Commun.*, 2013, **49**, 4720–4739.
6 E. W. Price and C. Orvig, *Chem. Soc. Rev.*, 2014, **43**, 260–290.
7 X. Wang, M. de G. Jaraquemada-Peláez, Y. Cao, J. Pan, K.-S. Lin, B. O. Patrick and C. Orvig, *Inorg. Chem.*, 2019, **58**, 2275–2285.

8 X. Wang, M. de G. Jaraquemada-Peláez, C. Rodríguez-Rodríguez, Y. Cao, C. Buchwalder, N. Choudhary, U. Jermilova, C. F. Ramogida, K. Saatchi, U. O. Häfeli, B. O. Patrick and C. Orvig, *J. Am. Chem. Soc.*, 2018, **140**, 15487–15500.
9 N. Choudhary, A. Dimmling, X. Wang, L. Southcott, V. Radchenko, B. O. Patrick, P. Comba and C. Orvig, *Inorg. Chem.*, 2019, **58**, 8685–8693.
10 N. Choudhary, M. de G. Jaraquemada-Peláez, K. Zarschler, X. Wang, V. Radchenko, M. Kubeil, H. Stephan and C. Orvig, *Inorg. Chem.*, 2020, **59**, 5728–5741.
11 X. Wang, M. de G. Jaraquemada-Peláez, C. Rodriguez-Rodriguez, J. Pan, Y. Wang, K. Saatchi, U. O. Ha, K. Lin and C. Orvig, *Inorg. Chem.*, 2020, **59**, 4895–4908.
12 K. Soroka, R. S. Vithanage, D. A. Phillips, B. Walker and P. K. Dasgupta, *Anal. Chem.*, 1987, **59**, 629–636.
13 K. F. Sugawara, H. H. Weetall and G. D. Schucker, *Anal. Chem.*, 1974, **46**, 489–492.
14 V. Prachayasittikul, S. Prachayasittikul, S. Ruchirawat and V. Prachayasittikul, *Drug Des., Dev. Ther.*, 2013, **7**, 1157–1178.
15 Y. Song, H. Xu, W. Chen, P. Zhan and X. Liu, *MedChemComm*, 2015, **6**, 61–74.
16 S. H. Chan, C. H. Chui, S. W. Chan, S. H. L. Kok, D. Chan, M. Y. T. Tsoi, P. H. M. Leung, A. K. Y. Lam, A. S. C. Chan, K. H. Lam and J. C. O. Tang, *ACS Med. Chem. Lett.*, 2013, **4**, 170–174.
17 G. Karpińska, A. P. Mazurek and J. C. Dobrowolski, *J. Mol. Struct.: THEOCHEM*, 2010, **961**, 101–106.
18 M. A. Green and J. C. Huffman, *J. Nucl. Med.*, 1988, **29**, 417.
19 M. Roca, E. F. J. de Vries, F. Jamar, O. Israel and A. Signore, *Eur. J. Nucl. Med. Mol. Imaging*, 2010, **37**, 835–841.
20 E. Schell-Frederick, J. Frühling, P. Van Der Auwera, Y. Van Laethem and J. Klastersky, *Cancer*, 1984, **54**, 817–824.
21 C. M. Intenzo, A. G. Desai, M. L. Thakur and C. H. Park, *J. Nucl. Med.*, 1987, **28**, 438–441.
22 P. Gawne, F. Man, J. Fonslet, R. Radia, J. Bordoloi, M. Cleveland, P. Jimenez-Royo, A. Gabizon, P. J. Blower, N. Long and R. T. M. De Rosales, *Dalton Trans.*, 2018, **47**, 9283–9293.
23 S. M. Valiahdi, P. Heffeter, M. A. Jakupec, R. Marculescu, W. Berger, K. Rappersberger and B. K. Keppler, *Melanoma Res.*, 2009, **19**, 283–293.
24 N. Sato, H. Wu, K. O. Asiedu, L. P. Szajek, G. L. Griffiths and P. L. Choyke, *Radiology*, 2015, **275**, 490–500.
25 P. Charoenphun, L. K. Meszaros, K. Chuamsaamarkkee, E. Sharif-Paghaleh, J. R. Ballinger, T. J. Ferris, M. J. Went, G. E. D. Mullen and P. J. Blower, *Eur. J. Nucl. Med. Mol. Imaging*, 2015, **42**, 278–287.
26 P. J. Gawne, F. Clarke, K. Turjeman, A. P. Cope, N. J. Long, Y. Barenholz, S. Y. A. Terry and R. T. M. de Rosales, *Theranostics*, 2020, **10**, 3867–3879.
27 K. O. Asiedu, M. Ferdousi, P. T. Ton, S. S. Adler, P. L. Choyke and N. Sato, *EJNMMI Res.*, 2018, **8**, 109.
28 J. R. Dilworth and S. I. Pascu, *Chem. Soc. Rev.*, 2018, **47**, 2554–2571.
29 M. A. Deri, B. M. Zeglis, L. C. Francesconi and J. S. Lewis, *Nucl. Med. Biol.*, 2013, **40**, 3–14.
30 E. W. Price, J. F. Cawthray, G. A. Bailey, C. L. Ferreira, E. Boros, M. J. Adam and C. Orvig, *J. Am. Chem. Soc.*, 2012, **134**, 8670–8683.
31 S. Poty, L. C. Francesconi, M. R. McDevitt, M. J. Morris and J. S. Lewis, *J. Nucl. Med.*, 2018, **59**, 878–884.
32 W. Y. Hsieh and S. Liu, *Inorg. Chem.*, 2004, **43**, 6006–6014.
33 P. Gans, A. Sabatini and A. Vacca, *Talanta*, 1996, **43**, 1739–1753.
34 P. Gans, A. Sabatini and A. Vacca, *Ann. Chim.*, 1999, **89**, 45–49.
35 L. Alderighi, P. Gans, A. Ienco, D. Peters, A. Sabatini and A. Vacca, *Coord. Chem. Rev.*, 1999, **184**, 311–318.
36 W. R. Harris, C. J. Carrano and K. N. Raymond, *J. Am. Chem. Soc.*, 1979, **101**, 2213–2214.
37 É. A. Enyedy, O. Dömötör, E. Varga, T. Kiss, R. Trondl, C. G. Hartinger and B. K. Keppler, *J. Inorg. Biochem.*, 2012, **117**, 189–197.
38 Y. Toporivska and E. Gumienna-Kontecka, *J. Inorg. Biochem.*, 2019, **198**, 110753.
39 M. Sturzbecher-Hoehne, T. A. Choi and R. J. Abergel, *Inorg. Chem.*, 2015, **54**, 3462–3468.
40 C. Buchwalder, M. de G. Jaraquemada-Peláez, J. Rousseau, H. Merkens, C. Rodríguez-Rodríguez, C. Orvig, F. Bénard, P. Schaffer, K. Saatchi and U. O. Häfeli, *Inorg. Chem.*, 2019, **58**, 14667–14681.
41 L. Li, M. de G. Jaraquemada-Peláez, H. T. Kuo, H. Merkens, N. Choudhary, K. Gitschtaler, U. Jermilova, N. Colpo, C. Uribe-Munoz, V. Radchenko, P. Schaffer, K. S. Lin, F. Bénard and C. Orvig, *Bioconjugate Chem.*, 2019, **30**, 1539–1553.
42 E. K. Sarbisheh, A. K. Salih, S. J. Raheem, J. S. Lewis and E. W. Price, *Inorg. Chem.*, 2020, **59**, 11715–11727.
43 P. Comba, U. Jermilova, C. Orvig, B. O. Patrick, C. F. Ramogida, K. Rück, C. Schneider and M. Starke, *Chem. – Eur. J.*, 2017, **23**, 15945–15956.
44 K. Arane, MSc Thesis, University of British Columbia, 2015.
45 O. K. Abou-Zied, N. Al-Lawatia, M. Elstner and T. B. Steinbrecher, *J. Phys. Chem. B*, 2013, **117**, 1062–1074.
46 É. A. Enyedy, O. Dömötör, K. Bali, A. Hetényi, T. Tuccinardi and B. K. Keppler, *J. Biol. Inorg. Chem.*, 2015, **20**, 77–88.
47 A. A. Hummer, C. Bartel, V. B. Arion, M. A. Jakupec, W. Meyer-Klaucke, T. Geraki, P. D. Quinn, A. Mijovilovich, B. K. Keppler and A. Rompel, *J. Med. Chem.*, 2012, **55**, 5601–5613.
48 G. Gran, *Analyst*, 1952, **77**, 661.
49 C. F. Baes Jr. and R. E. Mesmer, *The Hydrolysis of Cations*, John Wiley & Sons, New York, 1976.
50 C. F. Baes Jr. and R. E. Mesmer, *Am. J. Sci.*, 1981, **281**, 935–962.
51 M. J. Frisch, G. W. Trucks, H. B. Schlegel, G. E. Scuseria, M. A. Robb, J. R. Cheeseman, G. Scalmani, V. Barone, G. A. Petersson, H. Nakatsuji, X. Li, M. Caricato, A. V. Marenich, J. Bloino, B. G. Janesko, R. Gomperts, B. Mennucci, H. P. Hratchian, J. V. Ortiz, A. F. Izmaylov,

J. L. Sonnenberg, D. Williams-Young, F. Ding, F. Lipparini, F. Egidi, J. Goings, B. Peng, A. Petrone, T. Henderson, D. Ranasinghe, V. G. Zakrzewski, J. Gao, N. Rega, G. Zheng, W. Liang, M. Hada, M. Ehara, K. Toyota, R. Fukuda, J. Hasegawa, M. Ishida, T. Nakajima, Y. Honda, O. Kitao, H. Nakai, T. Vreven, K. Throssell, J. A. J. Montgomery, J. E. Peralta, F. Ogliaro, M. J. Bearpark, J. J. Heyd, E. N. Brothers, K. N. Kudin, V. N. Staroverov, T. A. Keith, R. Kobayashi, J. Normand, K. Raghavachari, A. P. Rendell, J. C. Burant, S. S. Iyengar, J. Tomasi, M. Cossi, J. M. Millam, M. Klene, C. Adamo, R. Cammi, J. W. Ochterski, R. L. Martin, K. Morokuma, O. Farkas, J. B. Foresman and D. J. G. Fox, *Gaussian 16, Revision C.01*, Gaussian, Inc., Wallingford, CT, 2016.

52 X. Li and M. J. Frisch, *J. Chem. Theory Comput.*, 2006, **2**, 835–839.

53 C. Adamo and V. Barone, *J. Chem. Phys.*, 1999, **110**, 6158–6170.

54 S. Grimme, S. Ehrlich and L. Goerigk, *J. Comput. Chem.*, 2011, **32**, 1456–1465.

55 S. Grimme, J. Antony, S. Ehrlich and H. Krieg, *J. Chem. Phys.*, 2010, **132**, 154104.

56 D. G. A. Smith, L. A. Burns, K. Patkowski and C. D. Sherrill, *J. Phys. Chem. Lett.*, 2016, **7**, 2197–2203.

57 F. Weigend and R. Ahlrichs, *Phys. Chem. Chem. Phys.*, 2005, **7**, 3297–3305.

58 D. Andrae, U. Haeussermann, M. Dolg, H. Stoll and H. Preuss, *Theor. Chim. Acta*, 1990, **77**, 123–141.

59 B. Metz, H. Stoll and M. Dolg, *J. Chem. Phys.*, 2000, **113**, 2563–2569.

60 X. Cao and M. Dolg, *J. Chem. Phys.*, 2001, **115**, 7348–7355.

61 X. Cao and M. Dolg, *J. Mol. Struct.: THEOCHEM*, 2002, **581**, 139–147.

62 K. L. Schuchardt, B. T. Didier, T. Elsethagen, L. Sun, V. Gurumoorthi, J. Chase, J. Li and T. L. Windus, *J. Chem. Inf. Model.*, 2007, **47**, 1045–1052.

63 B. P. Pritchard, D. Altarawy, B. Didier, T. D. Gibson and T. L. Windus, *J. Chem. Inf. Model.*, 2019, **59**, 4814–4820.

64 D. Feller, *J. Comput. Chem.*, 1996, **17**, 1571–1586.

65 J. Vícha, M. Patzschke and R. Marek, *Phys. Chem. Chem. Phys.*, 2013, **15**, 7740–7754.

66 M. Bühl, C. Reimann, D. A. Pantazis, T. Bredow and F. Neese, *J. Chem. Theory Comput.*, 2008, **4**, 1449–1459.

67 J. Vícha, J. Novotný, M. Straka, M. Repisky, K. Ruud, S. Komorovsky and R. Marek, *Phys. Chem. Chem. Phys.*, 2015, **17**, 24944–24955.

68 M. M. Quintal, A. Karton, M. A. Iron, A. D. Boese and J. M. L. Martin, *J. Phys. Chem. A*, 2006, **110**, 709–716.

69 S. Dohm, A. Hansen, M. Steinmetz, S. Grimme and M. P. Checinski, *J. Chem. Theory Comput.*, 2018, **14**, 2596–2608.

70 K. N. Kirschner, D. Reith and W. Heiden, *Soft Mater.*, 2020, **18**, 200–214.

71 A. Bauzá, D. Quiñonero, P. M. Deyaì and A. Frontera, *J. Phys. Chem. A*, 2013, **117**, 2651–2655.

72 L. Martinez, R. Andrade, E. G. Birgin and J. M. Martinez, *J. Comput. Chem.*, 2009, **30**, 2157–2164.

73 R. Dennington, T. A. Keith and J. M. Millam, *GaussView, Version 6.0.16*, Semichem Inc. Shawnee Mission KS, 2016.

74 M. D. Hanwell, D. E. Curtis, D. C. Lonie, T. Vandermeersch, E. Zurek and G. R. Hutchison, *J. Cheminf.*, 2012, **4**, 17.

